Probabilistic Engineering Mechanics 28 (2012) 176–184

Contents lists available at SciVerse ScienceDirect

Probabilistic Engineering Mechanics

journal homepage: www.elsevier.com/locate/probengmech

Variability response functions for stochastic systems under dynamic excitations

Vissarion Papadopoulos, Odysseas Kokkinos *

Institute of Structural Analysis and Seismic Research, National Technical University of Athens, 9 Iroon Polytechneiou, Zografou Campus, Athens 15780, Greece

ARTICLE INFO

Article history:
Received 14 June 2011
Received in revised form
13 July 2011
Accepted 17 August 2011
Available online 31 August 2011

Keywords:
Dynamic variability response functions
Stochastic finite element analysis
Upper bounds
Stochastic dynamic systems

ABSTRACT

The concept of variability response functions (*VRF*s) is extended in this work to linear stochastic systems under dynamic excitations. An integral form for the variance of the dynamic response of stochastic systems is considered, involving a Dynamic *VRF* (*DVRF*) and the spectral density function of the stochastic field modeling the uncertain system properties. As in the case of linear stochastic systems under static loads, the independence of the *DVRF* to the spectral density and the marginal probability density function of the stochastic field modeling the uncertain parameters is assumed. This assumption is here validated with brute-force Monte Carlo simulations. The uncertain system property considered is the inverse of the elastic modulus (flexibility). The same integral expression can be used to calculate the mean response of a dynamic system using a Dynamic Mean Response Function (*DMRF*) which is a function similar to the *DVRF*. These integral forms can be used to efficiently compute the mean and variance of the transient system response together with time dependent spectral-distribution-free upper bounds. They also provide an insight into the mechanisms controlling the dynamic mean and variability system response.

1. Introduction

Over the past two decades a lot of research has been dedicated to the stochastic analysis of structural systems involving uncertain parameters in terms of material or geometry with the implementation of stochastic finite element methodologies (SFEM) to numerically solve the stochastic partial differential equations (PDEs) governing the respective problems. The most commonly used SFEM methods are expansion/perturbation-based [1,2] and Galerkin-based Spectral SFEM (SSFEM) approaches [3]. Although such methods have proven to be highly accurate and computationally efficient for a variety of problems, there is still a wide range of problems in stochastic mechanics involving combinations of strong non-linearities and/or large variations of system properties as well as non-Gaussian system properties that can be solved with reasonable accuracy only through a computationally expensive Monte Carlo simulation approach [1,4–6], limited works deal with the dynamic propagation of system uncertainties, most of them reducing the stochastic dynamic PDEs to a linear random eigenvalue problem [7,8].

In all aforementioned cases, the spectral/correlation characteristics and the marginal probability distribution function (pdf) of the stochastic fields describing the uncertain system parameters are required in order to estimate the response variability of a stochastic static or dynamic system. As there is usually a lack of experimental data for the quantification of such probabilistic quantities, a sensitivity analysis with respect to various stochastic parameters is often implemented. In this case, however, the problems that arise are the increased computational effort, the lack of insight on how these parameters control the response variability of the system and the inability to determine bounds of the response variability.

In this framework and to tackle the aforementioned issues, the concept of the variability response function (*VRF*) was proposed in the late 1980s [9], along with different aspects and applications of the *VRF* [10,11]. A development of this approach was presented in a series of papers [12–14], where the existence of closed-form integral expressions for the variance of the response displacement of the form

$$Var[u] = \int_{-\infty}^{\infty} VRF(\kappa, \sigma_{ff}) S_{ff}(\kappa) \mathrm{d}\kappa \tag{1}$$

was demonstrated for linear stochastic systems under static loads using a flexibility-based formulation. The basic difference of this approach with respect to previous work is that by using a flexibility-based formulation, no approximations were involved in the derivation of the resulting integral expression in Eq. (1). It was shown that the *VRF* depends on standard deviation σ_{ff} but appears to be independent of the functional form of the spectral density function $S_{ff}(\kappa)$ modeling the inverse of the elastic modulus. The existence however of this integral expression had to be conjectured for statically indeterminate as well as for general stochastic finite element systems. A rigorous proof of such existence is

* Corresponding author.
E-mail addresses: vpapado@central.ntua.gr (V. Papadopoulos), okokki@central.ntua.gr (O. Kokkinos).

0266-8920/$ – see front matter © 2011 Elsevier Ltd. All rights reserved.
doi:10.1016/j.probengmech.2011.08.002

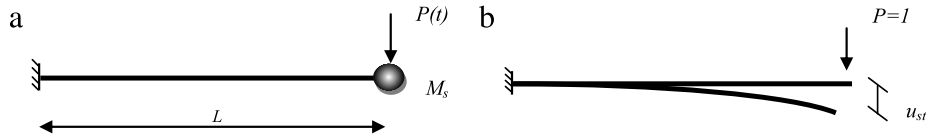

Fig. 1. One degree of freedom oscillator: (a) Geometry and loading (b) Static displacement for unit load.

available only for statically determinate systems for which *VRF* is independent of σ_{ff} as well [12]. Further investigations [15] verified the aforementioned results but showed that *VRF* has a slight dependence on the marginal pdf of the stochastic field modeling the flexibility. In [14], results were presented for general linear stochastic finite element systems including beams, space frames, plane stress and shell-type structures under static loads. Another important extension of the concept of *VRF* has been recently drawn [16] to determine effective material properties in homogenization problems.

The present paper extends the aforementioned approach to linear statically determinate stochastic systems under dynamic excitations. Although the derivation of an analytic expression for the variability response function of the dynamic system (*DVRF*), if possible at all, is extremely cumbersome, a numerical computation of the *DVRF* can be easily achieved to provide results for the variance time history of the dynamic system response. As in previous works [12–14], the existence of the *DVRF* and an integral form expression similar to Eq. (1) has to be conjectured. This assumption is numerically validated by comparing the results from Eq. (1) with brute force Monte Carlo simulations. It is demonstrated that the *DVRF* is highly dependent on the standard deviation σ_{ff} of the inverse of the elastic modulus and, based on numerical evidence further presented but, to this point, not to a full proof verification technique, appears to be almost independent of the functional form of $S_{ff}(\kappa)$ as well as of the marginal *pdf* of the flexibility. In addition, an integral expression similar to that of Eq. (1) is proposed for the mean system response involving a Dynamic Mean Response Function (*DMRF*), which is a function similar to the *DVRF*.

Both integral forms for the mean and variance can be used to efficiently compute the first and second order statistics of the transient system response with reasonable accuracy, together with time dependent spectral-distribution-free upper bounds. They also provide an insight into the mechanisms controlling the uncertainty propagation with respect to both space and time and in particular the mean and variability time histories of the stochastic system dynamic response.

2. Dynamic analysis of a stochastic single degree of freedom oscillator

For the single degree of freedom statically determinate stochastic oscillator of length L and mass M_s in Fig. 1(a), loaded with a dynamic deterministic load $P(t)$, the inverse of the elastic modulus is considered to vary randomly along the length of the beam according to the following expression:

$$\frac{1}{E(x)} = F_0(1 + f(x)) \tag{2}$$

where $E(x)$ is the elastic modulus, F_0 is the mean value of the inverse of $E(x)$, and $f(x)$ is a zero-mean homogeneous stochastic field modeling the variation of $1/E(x)$ around its mean value F_0.

The displacement time history $u(t)$ of the oscillator can be derived from the solution of Duhamel's integral:

$$u(t) = \frac{1}{\omega_D}\int_0^t P(\tau)\mathrm{e}^{-\xi\omega(t-\tau)}\sin(\omega_D(t-\tau))\mathrm{d}\tau \tag{3}$$

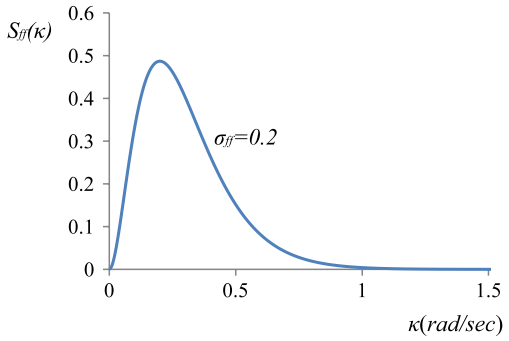

Fig. 2. Spectral density function for stochastic field $f(x)$ standard deviation $\sigma_{ff} = 0.2$.

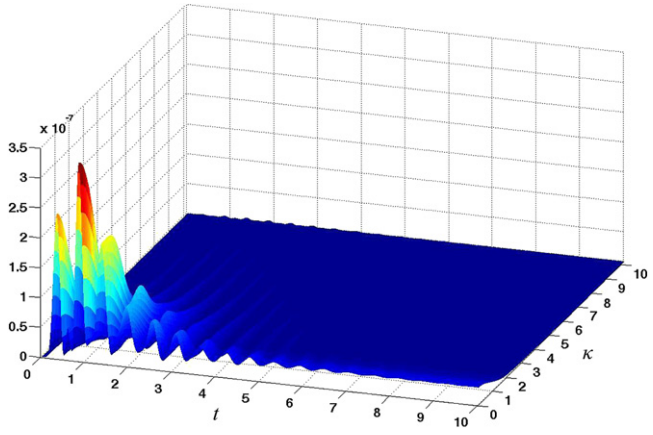

Fig. 3. 3D plot of *DVRF*, as a function of frequency κ (rad/m) and time t (s) for LC1 and $\sigma_{ff} = 0.2$.

where ξ is the damping ratio and $\omega_D = \omega\sqrt{1-\xi^2}$ with ω being the circular frequency of the system. Due to the system uncertainty in Eq. (2), the circular frequency ω is a random variable given by the following relation:

$$\omega = \sqrt{k/M_s} \tag{4}$$

where k is the stiffness of the oscillator which can be derived from the static displacement of the oscillator for a unit static deterministic load at the end of the beam (Fig. 1(b)) as follows:

$$k = \frac{1}{u_{st}} = \left[-\frac{F_0}{I}\int_0^L (x-\alpha)M(\alpha)(1+f(\alpha))\mathrm{d}\alpha\right]^{-1} \tag{5}$$

where I is the moment of inertia of the beam and $M(\alpha)$ is the moment at position α.

In the general case where the load is arbitrary and the system is initially at rest, the deterministic displacement at the right end of the beam can be derived by numerically solving Duhamel's integral. In the special case of a sinusoidal $P(t) = P_0\sin(\bar{\omega}t)$ the solution of Eq. (3) leads to the following expression for $u(t)$:

$$u(t) = u_0(t) + u_p(t) \tag{6}$$

where

$$u_0(t) = \mathrm{e}^{-\xi\omega t}(A\sin\omega_D t + B\cos\omega_D t) \tag{7a}$$

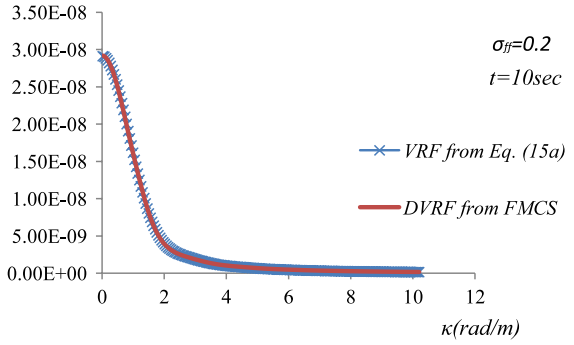

Fig. 4. Values of *VRF* for static load P_0 and *DVRF* for constant load $P(t) = P_0$ at $t = 10$ s.

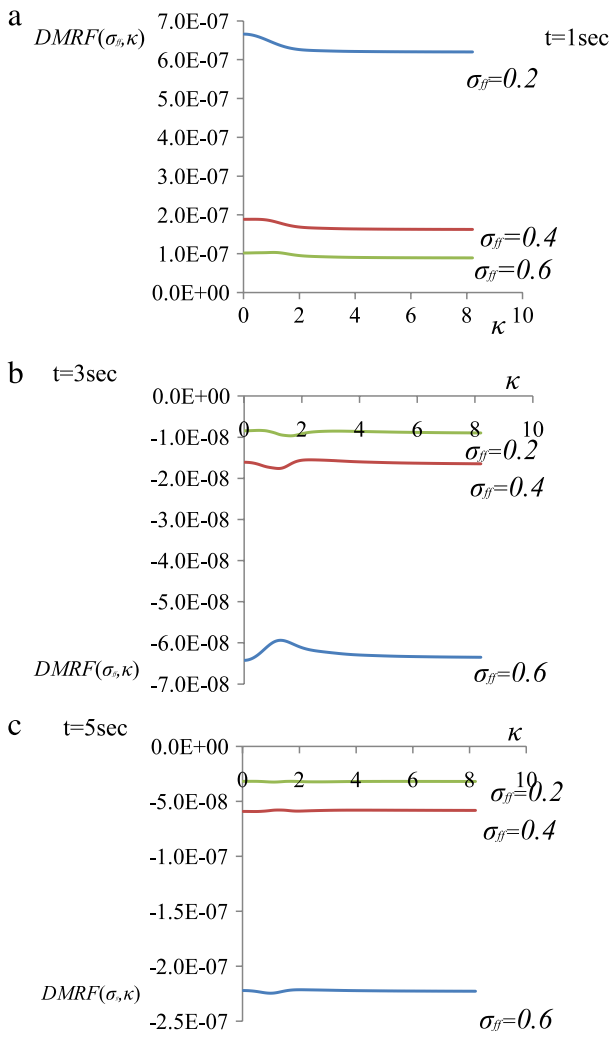

Fig. 5. *DMRF* as a function of σ_{ff} for (a) $t = 1$ s, (b) $t = 3$ s and (c) $t = 5$ s.

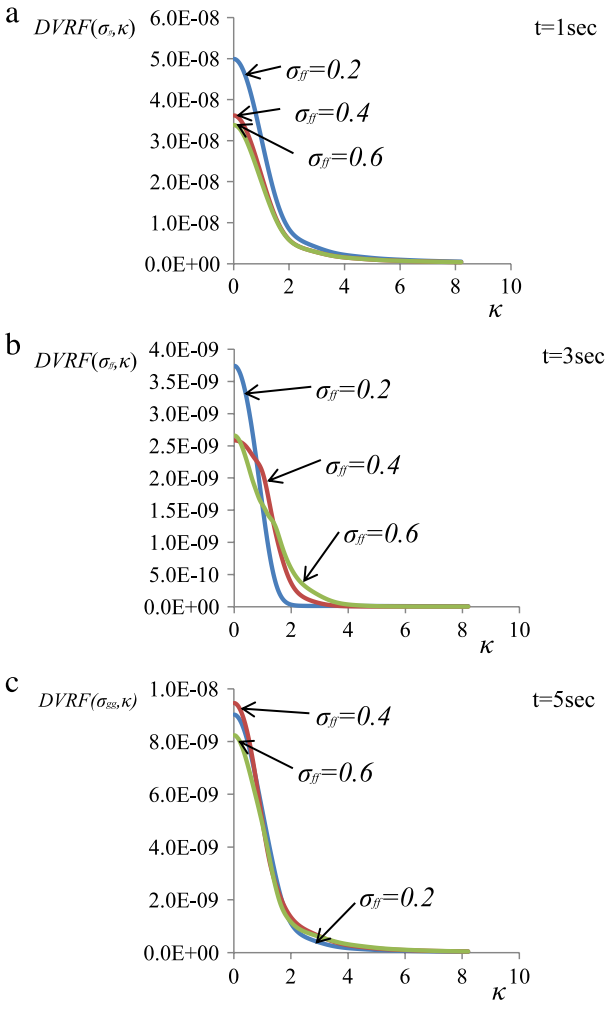

Fig. 6. *DVRF* as a function of σ_{ff} for (a) $t = 1$ s, (b) $t = 3$ s and (c) $t = 5$ s.

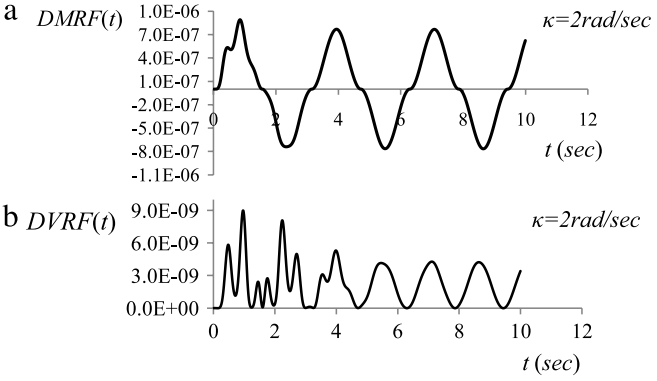

Fig. 7. *DMRF* (a) and *DVRF* (b) as a function of t for $\kappa = 2$ rad/s and $\sigma_{ff} = 0.2$.

$$u_p(t) = C_1 \sin \bar{\omega} t + C_2 \cos \bar{\omega} t \tag{7b}$$

$$A = \frac{P_0}{K} * \frac{1}{(1-\beta^2)^2 + (2\xi\beta)^2} * \frac{2\beta\xi^2 - (1-\beta^2)\beta}{\sqrt{1-\xi^2}} \tag{7c}$$

$$B = -\frac{P_0}{K} * \frac{2\xi\beta}{(1-\beta^2)^2 + (2\xi\beta)^2} \tag{7d}$$

$$C_1 = \frac{P_0}{K} * \frac{1}{(1-\beta^2)^2 + (2\xi\beta)^2}(1-\beta^2) \tag{7e}$$

$$C_2 = -\frac{P_0}{K} * \frac{1}{(1-\beta^2)^2 + (2\xi\beta)^2}(2\xi\beta) \tag{7f}$$

$$\beta = \bar{\omega}/\omega. \tag{7g}$$

In the trivial case in which a static load $P(t) = P_0$ is suddenly applied, the response displacement is given by

$$u(t) = \frac{P_0}{k}\left[1 - \left(\cos \omega_D t + \frac{\xi}{\sqrt{1-\xi^2}} \sin \omega_D t\right) e^{-\xi\omega t}\right]. \tag{7h}$$

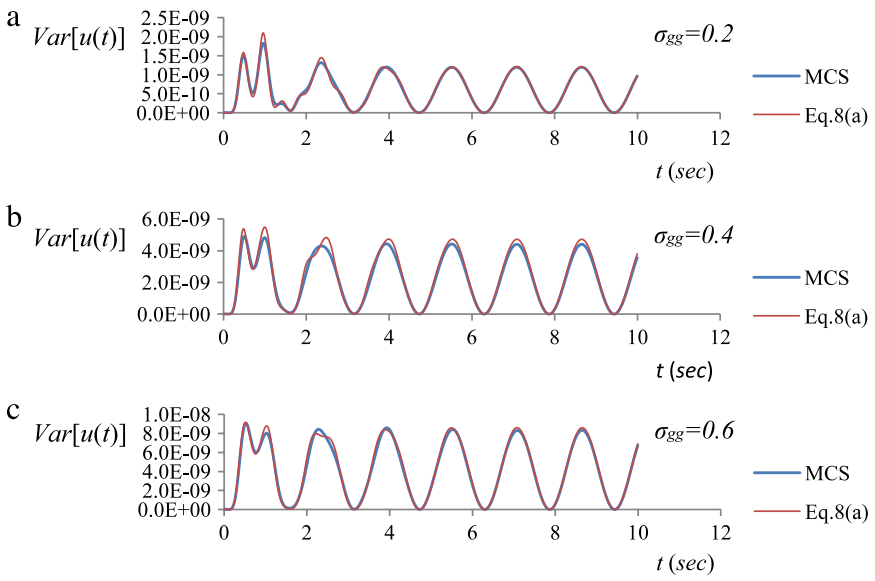

Fig. 8. Time histories of the variance of the response displacement for a truncated Gaussian field with (a) $\sigma_{gg} = 0.2$, (b) $\sigma_{gg} = 0.4$, and (c) $\sigma_{gg} = 0.6$. Comparison of results obtained from Eq. (8a) and MCS.

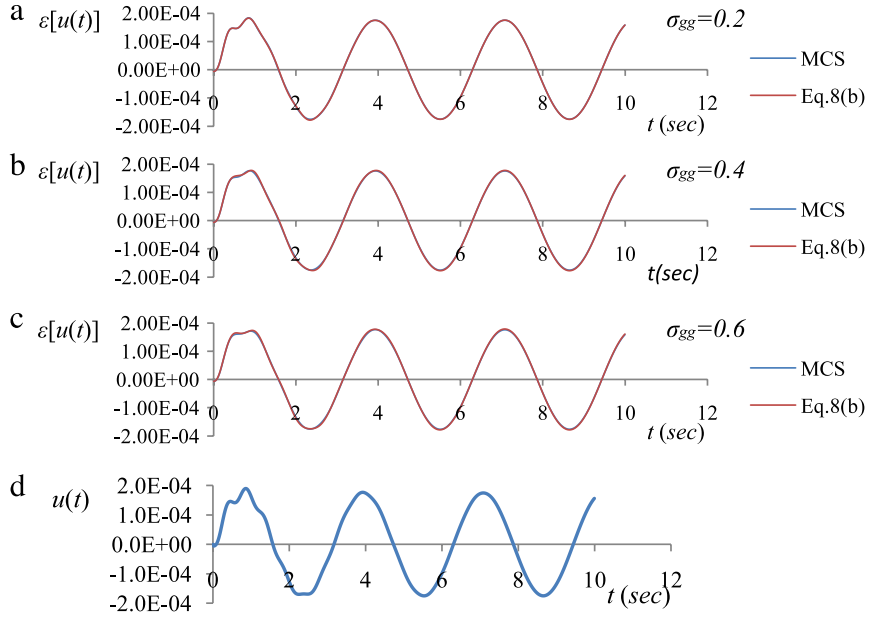

Fig. 9. Time histories of: (a) mean response displacement for a truncated Gaussian field with $\sigma_{gg} = 0.2$, (b) $\sigma_{gg} = 0.4$, (c) $\sigma_{gg} = 0.6$ and (d) the deterministic displacement. Comparison of results obtained from Eq. (8b) and MCS.

3. Response variance and mean value of the dynamic response

Following a procedure similar to the one presented in [12] for linear stochastic systems under static loading, it is possible to express the variance of the dynamic response of the stochastic system in the following integral form expression:

$$Var[u(t)] = \int_{-\infty}^{\infty} DVRF(t, \kappa, \sigma_{ff}) S_{ff}(\kappa) d\kappa \tag{8a}$$

where *DVRF* is the dynamic version of a *VRF*, assumed to be a function of deterministic parameters of the problem related to geometry, loads and (mean) material properties and the standard deviation σ_{ff} of the stochastic field that models the system flexibility. A similar integral expression can provide an estimate for the mean value of the dynamic response of the system using the Dynamic Mean Response Function (*DMRF*) [14]:

$$\varepsilon[u(t)] = \int_{-\infty}^{\infty} DMRF(t, \kappa, \sigma_{ff}) S_{ff}(\kappa) d\kappa. \tag{8b}$$

DMRF is assumed to be a function similar to the *DVRF* in the sense that it also depends on deterministic parameters of the problem as well as σ_{ff}. It is extremely difficult however, to prove that the *DVRF* (the same counts for *DMRF*) is independent (or even approximately independent) of the marginal pdf and the functional form of the power spectral density of the stochastic field $f(x)$. As in [12–14], the aforementioned assumptions are considered to form a conjecture which is numerically validated here by comparing the results from Eqs. (8a) and (8b) with brute force MCS.

The derivation of an analytic expression for the *DVRF* and *DMRF*, if possible at all, is an extremely cumbersome task. A numerical

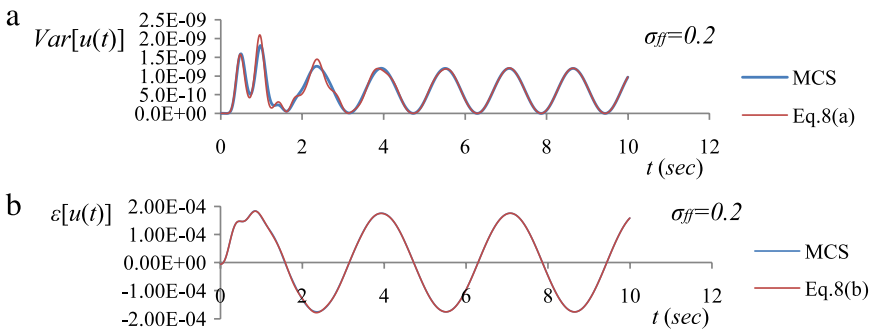

Fig. 10. Comparative results from Eq. (11) and MCS for a lognormal field with $\sigma_{ff} = 0.2$ for (a) the variance and (b) the mean of the response displacement time history.

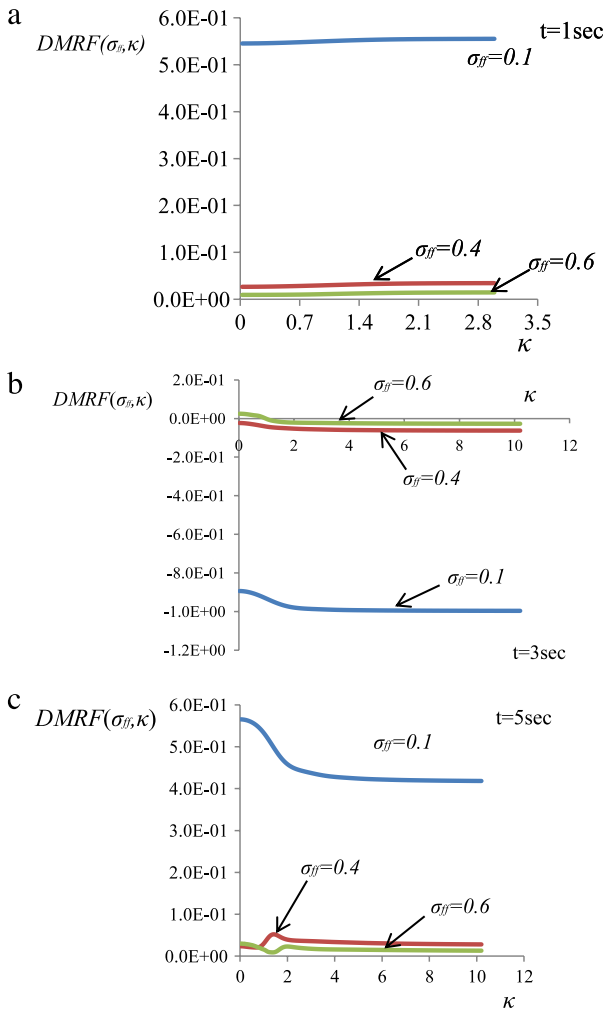

Fig. 11. *DMRF* as a function of σ_{ff} for (a) $t = 1$ s, (b) $t = 3$ s and (c) $t = 5$ s.

computation, however can be easily achieved, as described in the following section and then fed into Eqs. (8a) and (8b) to provide estimates of the mean and variance of the dynamic system response.

3.1. Numerical estimation of the DVRF and the DMRF using fast Monte Carlo simulation

The numerical estimation of *DVRF* and *DMRF* involves a fast Monte Carlo simulation (FMCS) whose basic idea is to consider the random field $f(x)$ as a random sinusoid [12,13] and plug its monochromatic power spectrum into Eqs. (8a) and (8b), in order to compute the respective mean and variance response at various wave numbers. The steps of the FMCS approach are the following:

(i) Generate N (10–20) sample functions of the random sinusoid given below with standard deviation σ_{ff} and wave number $\bar{\kappa}$ modeling the variation of the inverse of the elastic modulus $1/E$ around its mean F_0:

$$f_j(x) = \sqrt{2}\sigma_{ff}\cos(\bar{\kappa}x + \varphi_j) \tag{9}$$

where $j = 1, 2, \ldots, N$ and φ_j varies randomly under uniform distribution in the range $[0, 2\pi]$.

(ii) Using these N generated sample functions it is straightforward to compute their respective dynamic mean and response variance, $\varepsilon[u(t)]_{\bar{\kappa}}$ and $Var[u(t)]_{\bar{\kappa}}$, respectively for a given time step t.

(iii) The value of the *DMRF* at wave number $\bar{\kappa}$ can then be computed as follows

$$DMRF(t, \bar{\kappa}, \sigma_{ff}) = \frac{\varepsilon[u(t)]_{\bar{\kappa}}}{\sigma_{ff}^2} \tag{10a}$$

and likewise the value of the *DVRF* at wave number $\bar{\kappa}$

$$DVRF(t, \bar{\kappa}, \sigma_{ff}) = \frac{Var[u(t)]_{\bar{\kappa}}}{\sigma_{ff}^2}. \tag{10b}$$

Both previous equations are direct consequences of the integral expressions in Eqs. (8a) and (8b) in the case that the stochastic field becomes a random sinusoid.

(iv) Get *DMRF* and *DVRF* as a function of both time t and wave number κ by repeating previous steps for various wave numbers and different time steps. The entire procedure can be repeated for different values of the standard deviation σ_{ff} of the random sinusoid.

3.2. Bounds of the mean and variance of the dynamic response

Upper bounds on the mean and variance of the dynamic response of the stochastic system can be established directly from Eqs. (8a) and (8b), as follows:

$$\begin{aligned}\varepsilon[u(t)] &= \int_{-\infty}^{\infty} DMRF(t, \kappa, \sigma_{ff}) S_{ff}(\kappa)\mathrm{d}\kappa \\ &\le DMRF(t, \kappa^{\max}(t), \sigma_{ff})\sigma_{ff}^2\end{aligned} \tag{11a}$$

$$\begin{aligned}Var[u(t)] &= \int_{-\infty}^{\infty} DVRF(t, \kappa, \sigma_{ff}) S_{ff}(\kappa)\mathrm{d}\kappa \\ &\le DVRF(t, \kappa^{\max}(t), \sigma_{ff})\sigma_{ff}^2\end{aligned} \tag{11b}$$

where $\kappa^{\max}(t)$ is the wave number at which *DMRF* and *DVRF*, corresponding to a given time step t and value of σ_{ff}, reach their maximum value. An envelope of time evolving upper bounds on the mean and variance of the dynamic system response can be extracted from Eqs. (11a) and (11b). As in the case of linear

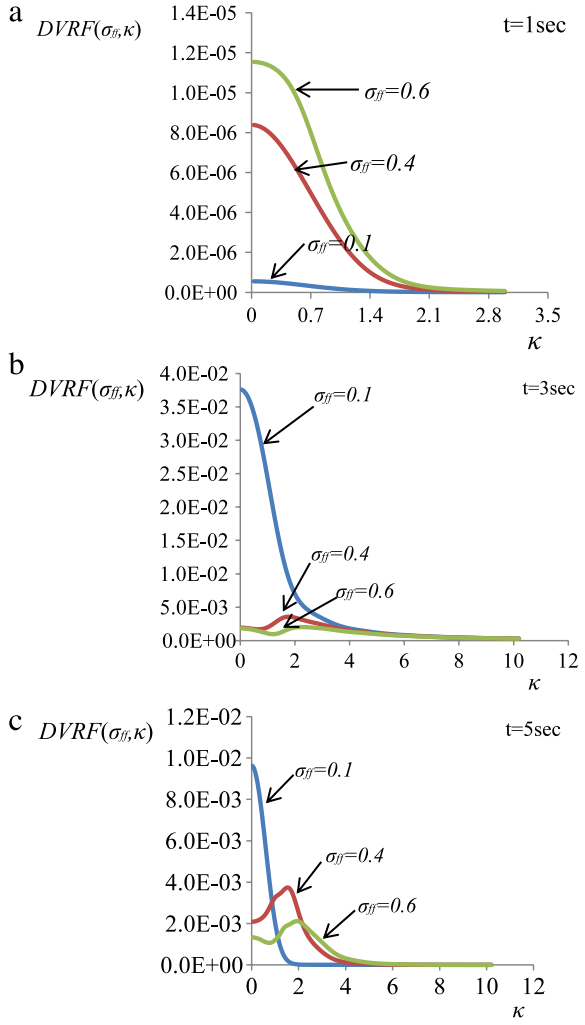

Fig. 12. *DVRF* as a function of σ_{ff} for (a) $t = 1$ s, (b) $t = 3$ s and (c) $t = 5$ s.

stochastic systems under static loads [12–14], this envelope is physically realizable since the form of the stochastic field that produces it is the random sinusoid of Eq. (9) with $\bar{\kappa} = \kappa^{\max}(t)$.

4. Numerical example

For the cantilever beam shown in Fig. 1 with length $L = 4$ m, the inverse of the modulus of elasticity is assumed to vary randomly along its length according to Eq. (2) with $F_0 = (1.25\times10^8\ \text{kN/m})^{-1}$ and $I = 0.1\ \text{m}^4$. A concentrated mass $M_s = 3.715 \times 10^3$ kg is assumed at the right end of the beam. The damping ratio is taken as $\xi = 5\%$ and the mean eigenperiod of this one d.o.f oscillator is calculated at $T_0 = 0.5$ s.

Three load cases are considered: LC1 consisting of a constant load $P(t) = 100$, LC2 consisting of a concentrated dynamic periodic load $P(t) = 100\sin(\bar{\omega}t)$ and LC3 consisting of $P(t) = -M_s\ddot{U}_g(t)$ where $\ddot{U}_g(t)$ is the acceleration time history of the 1940 El Centro earthquake.

The spectral density function (*SDF*) of Fig. 2 was used for the modeling of the inverse of the elastic modulus stochastic field, given by:

$$S_{ff}(\kappa) = \frac{1}{4}\sigma^2 b^3\kappa^2 \mathrm{e}^{-b|\kappa|} \tag{12}$$

with $b = 10$ being a correlation length parameter.

In order to demonstrate the validity of the proposed methodology, a truncated Gaussian and a lognormal pdf were used to model $f(x)$. For this purpose, an underlying Gaussian stochastic

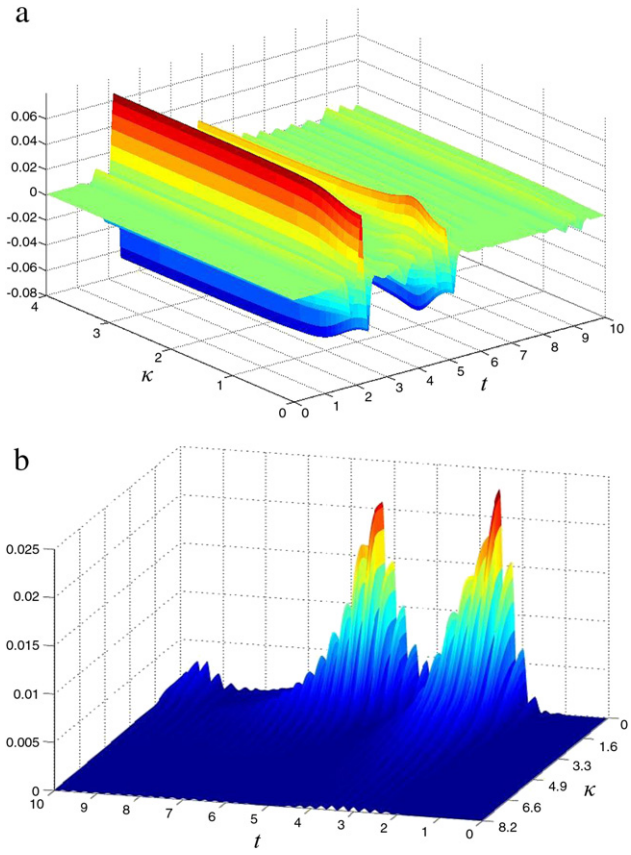

Fig. 13. 3D plots of (a) *DMRF* and (b) *DVRF*, as a function of frequency κ (rad/m) and time t (s) for LC3 and $\sigma_{ff} = 0.2$.

field denoted by $g(x)$ is generated using the spectral representation method [17] and the power spectrum of Eq. (12). The truncated Gaussian field $f_{\text{TG}}(x)$ is obtained by simply truncating $g(x)$ in the following way: $-0.9 \le g(x) \le 0.9$, while the lognormal $f_{\text{L}}(x)$ is obtained from the following transformation as a translation field [18]:

$$f_{\text{L}}(x) = F_{\text{L}}^{-1}\{G[g(x)]\}. \tag{13}$$

The *SDF* of the underlying Gaussian field in Eq. (12) and the corresponding spectral densities of the truncated Gaussian and the lognormal fields denoted $S_{f_{\text{TG}}f_{\text{TG}}}(\kappa)$ and $S_{f_{\text{L}}f_{\text{L}}}(\kappa)$, respectively, will be different. These are computed from the following formula

$$S_{f_if_i}(\kappa) = \frac{1}{2\pi L_x}\left|\int_0^{L_x} f_i(x)\mathrm{e}^{-\mathrm{i}\kappa x}\mathrm{d}x\right|^2; \quad i = \text{TG, L} \tag{14}$$

where L_x is the length of the sample functions of the non-Gaussian field modeling flexibility. As the sample functions of the non-Gaussian fields are non-ergodic, the estimation of power spectra in Eq. (14) is performed in an ensemble average sense [18].

LC1: constant load at the end of the beam

This load case scenario has been selected in order to further demonstrate the validity of the methodology and establish a logical continuation with previous studies related to the current work. In the case when the excitation is constant $P(t) = P_0$, and the load P_0 is suddenly applied, the response displacement is given by Eq. (7h). From this equation it can be seen that the solution degenerates to the static solution $u(t) = P_0/k$ as time t tends to infinity. Accordingly the *DVRF* should converge to the respective static *VRF* of a cantilever beam loaded with a concentrated load at

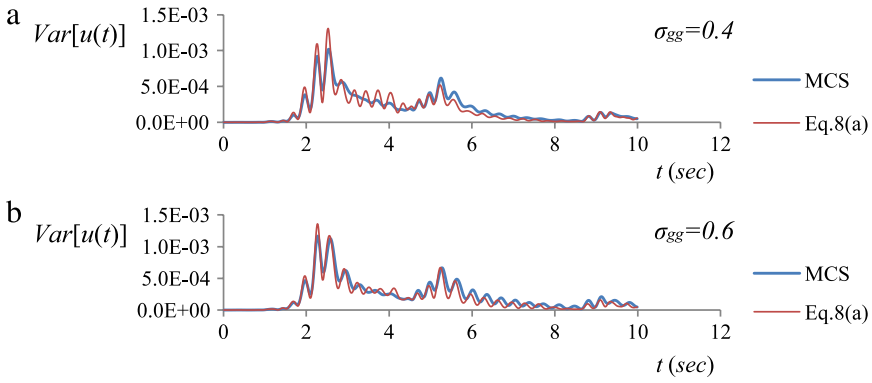

Fig. 14. Time histories of the variance of the response displacement for a truncated Gaussian field for (a) $\sigma_{gg} = 0.4$ and (b) $\sigma_{gg} = 0.6$. Comparison of results obtained from Eq. (8a) and MCS.

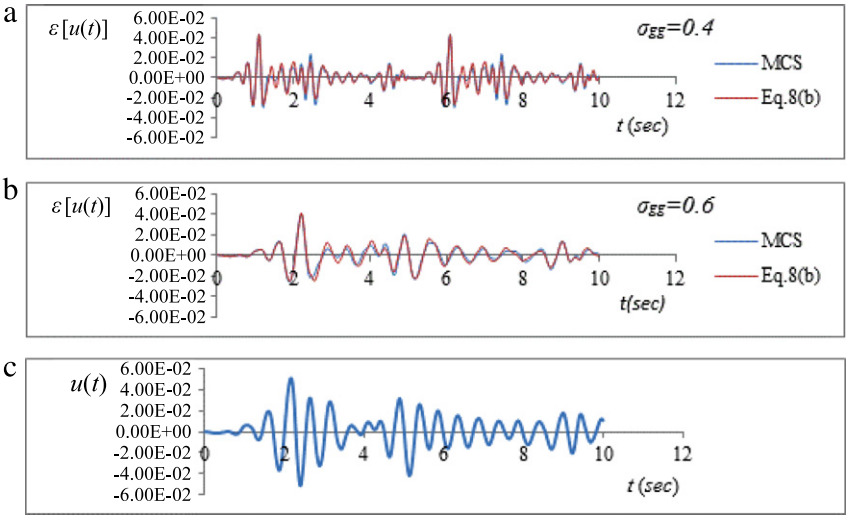

Fig. 15. Time histories of the mean response displacement for a truncated Gaussian field with (a) $\sigma_{gg} = 0.4$, (b) $\sigma_{gg} = 0.6$ and (c) of the deterministic response displacement. Comparison of results obtained from Eq. (8b) and MCS.

its end, given by Eq. (15) [12].

$$VRF(x,\kappa) = \left| \frac{F_0}{I} \int_0^x h(x,\xi) M(\xi) e^{i\kappa\xi} d\xi \right|^2 \tag{15a}$$

where $h(x,\xi)$ is the Green function of the beam given by

$$h(x,\xi) = x - \xi \tag{15b}$$

and $M(x)$ is the bending moment function given by

$$M(\xi) = -P_0(L-\xi). \tag{15c}$$

Validating the aforementioned expectations, Fig. 3 presents a 3D plot of the *DVRF* with an initial transient phase and afterward the phase where the system is almost at rest, while Fig. 4 presents the coinciding *VRF* and *DVRF* obtained from Eq. (15a) and *FMCS, respectively*, when the system has approached the stationary condition at $t = 10$ s and $\sigma_{ff} = 0.2$.

LC2: dynamic periodic load at the end of the beam

Figs. 5 and 6 present *DMRF* and *DVRF*, respectively, computed with FMCS for a periodic load with frequency $\bar{\omega} = 2$ and three different values of the standard deviation $\sigma_{ff} = 0.2$, $\sigma_{ff} = 0.4$ and $\sigma_{ff} = 0.6$. From these figures it can be observed that *DVRF* do not follow any particular pattern with respect to any increase or decrease of σ_{ff} in contrast to *DMRF* and to what has been observed in [13] for the corresponding static problem, albeit the mean and variability response increase as σ_{ff} increases, as shown below (Fig. 8). Fig. 7(a) and (b) present plots of *DMRF* and *DVRF* as a function of t for a fixed wave number $\kappa = 2$ and $\sigma_{ff} = 0.2$. From Figs. 5–7 it appears that *DMRF* and *DVRF* have a significant variation along the wave number κ axis and the time axis t. Both functions and especially *DVRF* have an initial transient phase and then appear to be periodic. It is reminded here that *DVRF* and *DMRF* are functions of the imposed dynamic loading. This explains the fact that they do not approach zero with t increasing, since the applied dynamic load is periodic with constant amplitude which does not decay.

Fig. 8(a)–(c) present comparatively the results of the computed response variance time histories using the integral expression of Eq. (8a) and MCS, for three different standard deviations of a truncated Gaussian stochastic field used for the modeling of flexibility. The underlying Gaussian field is modeled with the power spectral density of Eq. (12) and three different standard deviations $\sigma_{gg} = 0.2$, $\sigma_{gg} = 0.4$ and $\sigma_{gg} = 0.6$. The corresponding standard deviations of the truncated Gaussian field $f(x)$ are computed as $\sigma_{ff} = 0.2$, $\sigma_{ff} = 0.3912$ and $\sigma_{ff} = 0.5286$, respectively. Fig. 9(a)–(c), present the same results with Fig. 8 but for the mean response of the oscillator. The deterministic displacement time history is also plotted in Fig. 9(d) for comparison purposes. From these figures it can be observed that the mean and variability response time histories obtained with the integral expressions of Eqs. (8a) and (8b) are in close agreement with the corresponding MCS estimates. In all cases examined the maximum error in the computed $Var[u(t)]$, observed at the peak values of the variance, is less than 25%, while in all other time steps this error is less than 3%–4%. In the case of

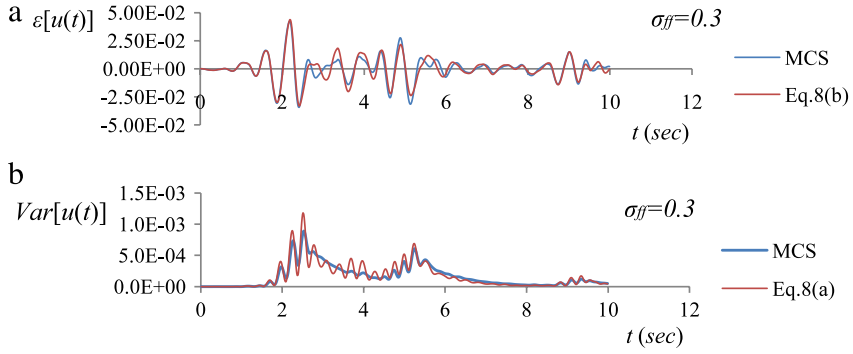

Fig. 16. Comparative results from Eq. (11) and MCS for a lognormal field with $\sigma_{ff} = 0.3$ for (a) the variance and (b) the mean of the response displacement time history.

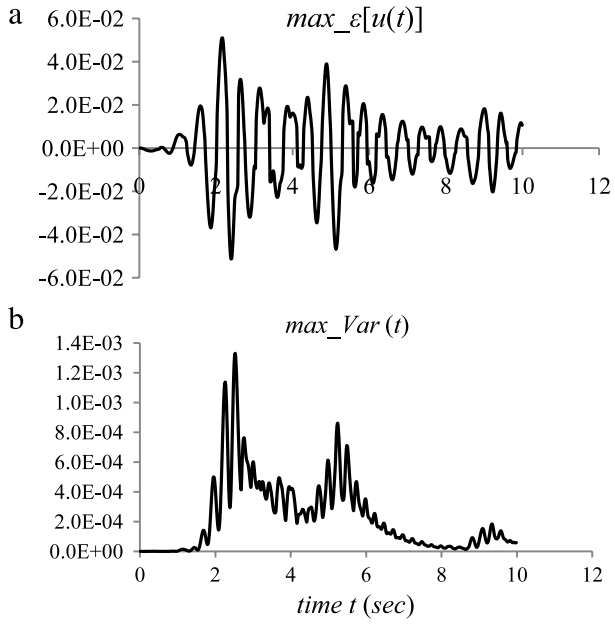

Fig. 17. Upper bounds on the (a) mean and (b) variance of the response displacement for LC3 and $\sigma_{gg} = 0.4$.

$\varepsilon[u(t)]$, the predictions of Eq. (8b) are almost identical to the ones obtained with MCS, with an error of less than 3% in all cases. From Fig. 9(a–d), it can be observed that in all cases, the mean response time history for all cases examined is almost identical to the deterministic one, with the exception of the first cycle where slight differences in the peak values are observed.

Fig. 10(a) and (b) repeat the same comparisons with the previous Figs. 8 and 9 but for the case of a lognormal stochastic field used for the modeling of flexibility with $\sigma_{ff} = 0.2$ and lower bound $l_b = -0.8$. The conclusions extracted previously for the case of truncated Gaussian fields also apply here (Fig. 10).

LC3: El Centro earthquake

Figs. 11 and 12 present plots of *DMRF* and *DVRF*, respectively, for the load case of the acceleration time history of the 1940 El Centro earthquake. As in the previous load case scenario, three different values of the standard deviation were used, $\sigma_{ff} = 0.2$, $\sigma_{ff} = 0.4$ and $\sigma_{ff} = 0.6$. From these figures it can again be observed that *DVRF* does not follow any pattern with respect to an increase or decrease of σ_{ff}, while in this case this is also observed for the *DMRF* at Fig. 11(c) for $t = 5$ s.

Fig. 13(a) and (b) present 3D plots of the *DMRF* and *DVRF* as a function of frequency κ and time t (s) for $\sigma_{ff} = 0.2$. From these figures, as well as from Figs. 11 and 12, it can be observed that again *DMRF* and *DVRF* have a significant variation in both κ and t axis, without being periodic in contrast to what has been observed in LC2. In addition, both *DMRF* and *DVRF* approach a zero value with time increasing due to the fact that ground accelerations decay and vanish after some time.

Fig. 14(a) and (b) present a comparison of the response variance computed with Eq. (8a) and MCS, in the case of a truncated Gaussian stochastic field modeling flexibility with $\sigma_{gg} = 0.4$ and 0.6, while Fig. 15(a) and (b) present the same results for the mean dynamic response of the stochastic oscillator along with the corresponding deterministic displacement time history (Fig. 15(c)). Fig. 16(a) and (b) repeat the same comparisons for the case of a lognormal stochastic field used for the modeling of flexibility and $\sigma_{ff} = 0.3$ and lower bound $l_b = -0.8$.

From the above figures it can be observed that, as in LC2, the mean and variability response time histories obtained with the integral expressions of Eqs. (8a) and (8b) are in close agreement with the corresponding MCS estimates, in all cases. Again, the maximum error in the computed $Var[u(t)]$ was observed at the peak values of the variance and is less than 25%, while in all other time steps this error is less than 3%–4%. In the case of $\varepsilon[u(t)]$, the predictions of Eq. (8b) are very close to the ones obtained with MCS, with an error of less than 3% in all cases. From Fig. 15(a–c), it can be observed that, in contrast to what was observed in LC2, the mean response time history differs significantly from the corresponding deterministic one, in terms of both frequencies and amplitudes.

Upper bounds on the mean and variance of the response of LC3

Spectral-distribution-free upper bounds on both the mean and variance of the response are obtained via Eqs. (11a) and (11b), respectively. Results of this calculation are presented in Fig. 16(a) and (b), in which the time dependent upper bounds on the mean and variance of the response displacement are plotted against time for a standard deviation $\sigma_{ff} = 0.4$.

Sensitivity analysis for LC3 using the integral expressions in Eqs. (8a) and (8b)

Finally, a sensitivity analysis is performed using Eqs. (8a) and (8b) at minimum computational cost, with respect to three different values of the correlation length parameter of the *SDF* in Eq. (12) and $\sigma_{ff} = 0.2$ (Figs. 17 and 18).

5. Concluding remarks

In the present work, dynamic variability response functions and dynamic mean response functions are obtained for a linear stochastic single d.o.f. oscillator with random material properties under dynamic excitation. The inverse of the modulus of elasticity was considered as the uncertain system parameter.

It is demonstrated that, as in the case of stochastic systems under static loading, *DVRF* and *DMRF* depend on the standard deviation of the stochastic field modeling the uncertain parameter but appear to be almost independent of its power spectral density and marginal *pdf*. The results obtained from the integral

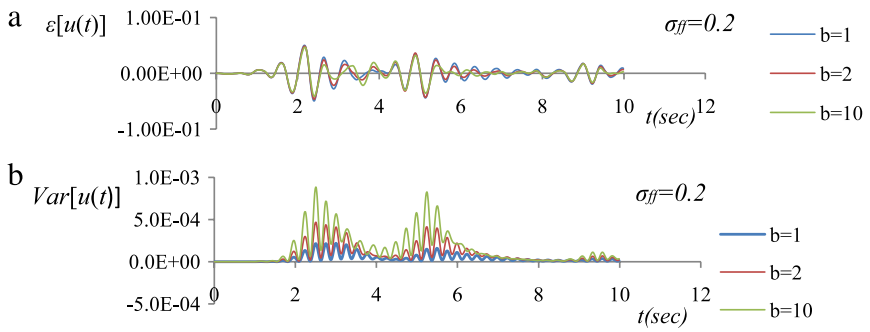

Fig. 18. (a) Mean and (b) variance time histories of the response displacement computed from Eqs. (8a) and (8b), respectively for three different values of the correlation length parameter b of the *SDF* in Eq. (12).

expressions are close to those obtained with MCS reaching a maximum error of the order of 20%–25%.

As in the case of stochastic systems under static loading, the *DVRF* and the *DMRF* provide us with an insight into the dynamic system sensitivity to the stochastic parameters and the mechanisms controlling the response mean and variability and their evolution in time.

References

[1] Liu WK, Belytschko T, Mani A. Probabilistic finite elements for nonlinear structural dynamics. Comput Methods Appl Mech Engrg 1986;56:61–86.
[2] Liu WK, Belytschko T, Mani A. Random field finite elements. Internat J Numer Methods Engrg 1986;23:1831–45.
[3] Ghanem R, Spanos PD. Stochastic finite elements: a spectral approach. 2nd ed. Berlin: Springer-Verlag; 1991. Dover Publications, NY, 2003.
[4] Grigoriu M. Evaluation of Karhunen–Loève, spectral and sampling representations for stochastic processes. J Engrg Mech (ASCE) 2006;132:179–89.
[5] Matthies HG, Brenner CE, Bucher CG, Guedes Soares C. Uncertainties in probabilistic numerical analysis of structures and solids — stochastic finite elements. Struct Saf 1997;19:283–336.
[6] Stefanou George. The stochastic finite element method: past, present and future. Comput Methods Appl Mech Eng 2009;198(9–12):1031–51.
[7] Ghosh D, Ghanem R, Red-Horse J. Analysis of eigenvalues and modal interaction of stochastic systems. AIAA J 2005;43(10):2196–201.
[8] Schueller GI. Model reduction and uncertainties in structural dynamics. In: Papadrakakis M, Stefanou G, Papadopoulos V, editors. Computational methods in stochastic dynamics. Springer; 2011.
[9] Shinozuka M. Structural response variability. J Engrg Mech 1987;113(6):825–42.
[10] Wall FJ, Deodatis G. Variability response functions of stochastic plane stress/strain problems. J Engrg Mech 1994;120(9):1963–82.
[11] Graham L, Deodatis G. Weighted integral method and variability response functions for stochastic plate bending problems. Struct Saf 1998;20:167–88.
[12] Papadopoulos V, Deodatis G, Papadrakakis M. Flexibility-based upper bounds on the response variability of simple beams. Comput Methods Appl Mech Eng 2005;194(12–16):1385–404. 8.
[13] Papadopoulos V, Deodatis G. Response variability of stochastic frame structures using evolutionary field theory. Comput Methods Appl Mech Engrg 2006;195(9–12):1050–74.
[14] Papadopoulos V, Papadrakakis M, Deodatis G. Analysis of mean response and response variability of stochastic finite element systems. Comput Meth Appl Mech Eng 2006;195(41–43):5454–71.
[15] Miranda M. On the response variability of beam structures with stochastic parameters. Ph.D. thesis. Columbia University; 2008.
[16] Arwade SR, Deodatis G. Variability response functions for effective material properties. Probab Engrg Mech 2011;26:174–81.
[17] Shinozuka M, Deodatis G. Simulation of stochastic processes by spectral representation. Appl Mech Rev 1991;44(4):191–203.
[18] Grigoriu M. Applied non-Gaussian processes: examples, theory, simulation, linear random vibration, and MATLAB solutions. Prentice Hall; 1995.